Optimization of graphene-functionalized polycaprolactone nanofibers: enhancing mechanical, thermal, and biocompatibility properties for biomedical applications

T. Sankar [a,*], T. K. Kannan [b], R. Rajasekar [c], N. Balakrishnan [b]
[a] *Department of Mechanical Engineering, Paavai College of Engineering, Namakkal, Tamilnadu, India-637018*
[b] *Department of Mechanical Engineering, Gnanamani College of Technology, Namakkal, Tamilnadu, India-637018*
[c] *Department of Mechanical Engineering, Kongu Engineering College, Erode, Tamilnadu, India-638060*

The development of biocompatible materials with enhanced properties is critical for biomedical applications. However, polycaprolactone (PCL), a widely used biodegradable polymer, exhibits insufficient mechanical and thermal properties for demanding applications. This study addresses the challenge by incorporating carboxyl-functionalized graphene (CFG) and hydroxyl-functionalized graphene (HFG) derivatives into PCL nanofibers using electrospinning. The objective is to optimize graphene content to improve the mechanical strength, thermal stability, and biocompatibility of the nanocomposites. Electrospun nanofibers with varying graphene concentrations (0.5, 1, and 2 wt%) were characterized for morphology, mechanical properties, thermal behavior, and cell viability. Results demonstrated that 1 wt% graphene content provided optimal performance, significantly enhancing tensile strength (5.5 MPa for CFG, 5.4 MPa for HFG) and Young's modulus while maintaining uniform, bead-free fibers. Thermal analysis revealed improved crystallinity and degradation temperature, while MTT assays showed superior cell viability (up to 93%) at 1 wt% graphene. These highlight the potential of PCL/graphene nanocomposites as high-performance biomaterials for tissue regeneration. Future research should explore in vivo performance and long-term biological effects to confirm their clinical viability.

(Received January 2, 2025; Accepted April 28, 2025)

Keywords: PCL nanocomposites, Electrospinning, Graphene, Mechanical properties, Biocompatibility

1. Introduction

Graphene has been widely researched for its superior mechanical, electrical, and thermal properties[1]. Functionalizing graphene with carboxyl (CFG) and hydroxyl (HFG) groups improves its compatibility with polymer matrices, allowing for better dispersion and stronger interfacial interactions[2]. The functional groups on graphene help avoid agglomeration and promote uniform distribution within the polymer. Electrospinning, a versatile and scalable technique, is used in this study to fabricate nanofibers from PCL/graphene composites. Electrospun fibers offer a high surface area, porous structure, and tunable mechanical properties[3].This study focuses on the incorporation of functionalized graphene derivatives into PCL to produce electrospun nanocomposite fibers with enhanced properties.

Despite extensive research on electrospinning and nanocomposites, the problem remains that the mechanical and thermal properties of PCL must be improved for practical biomedical applications, particularly when long-term structural integrity is required. Furthermore, while graphene's potential to enhance polymer properties is well-known, the optimal concentration of functionalized graphene to balance mechanical enhancement, thermal stability, and biocompatibility in PCL-based composites has not been clearly identified. Higher graphene content can sometimes lead to undesirable agglomeration, reducing the material's overall

*Corresponding author: ersankar.t@gmail.com
https://doi.org/10.15251/DJNB.2025.202.443

performance. This study addresses these challenges by investigating the effects of concentrations of CFG and HFG on the properties of PCL nanofibers[4].

Several studies have highlighted the ability of graphene to reinforce polymers, increasing their tensile strength, Young's modulus, and thermal stability. For example, previous research has demonstrated that incorporating small amounts of graphene into polymers like polylactic acid (PLA) or polyvinyl alcohol (PVA) can significantly improve their properties. Functionalization of graphene is a key step in enhancing its dispersion within polymer matrices, as pristine graphene often tends to agglomerate due to van der Waals forces. CFG and HFG, with their carboxyl and hydroxyl groups, can form hydrogen bonds with PCL, leading to better interaction and load transfer. However, the exact balance of graphene content required to optimize both mechanical properties and biocompatibility in PCL-based nanocomposites has not been extensively explored, which forms the core focus of this research[5].

The functionalized graphene derivatives provide additional bioactive sites for cell adhesion, thereby promoting cell proliferation, which is critical for the success of biomedical scaffolds[6]. The biocompatibility of the PCL/graphene composites must also be carefully evaluated to ensure that the improvements in mechanical and thermal properties do not compromise the material's interaction with biological systems[7].

This research presents several novelties, including the use of electrospun PCL nanofibers reinforced with carboxyl- and hydroxyl-functionalized graphene derivatives at various concentrations. While previous studies have incorporated graphene into polymers, the effect of these specific functionalized derivatives on PCL nanocomposites in terms of mechanical, thermal, and biological properties has not been thoroughly studied. The novelty of this study also lies in its comprehensive analysis of the optimal graphene content that enhances performance without compromising biocompatibility, which is crucial for clinical applications. In particular, the focus on both mechanical strength and biocompatibility simultaneously is a step forward in developing practical, multifunctional biomedical materials[8].

The objectives of this study are to (1) develop electrospun nanocomposites by incorporating CFG and HFG into a PCL matrix, (2) optimize the concentration of graphene derivatives and (3) assess the biocompatibility of these nanocomposites for potential biomedical applications. The study involves varying the concentration of functionalized graphene derivatives to investigate their effects[10]. This will allow the identification of the optimal graphene content that balances enhanced material properties with cell compatibility[9].

2. Materials and methods

The base material used in this study was PCL, a biodegradable, biocompatible. PCL's low melting point, slow degradation rate, and mechanical flexibility make it an ideal candidate for electrospinning and nanofiber fabrication. To ensure the success and reproducibility of the process, several precautions were observed. The polymer solution was prepared with appropriate viscosity, conductivity, and surface tension to allow stable jet formation and to prevent bead formation. Environmental conditions, such as temperature, humidity, and airflow, were carefully controlled, as they significantly influenced the morphology of the fibers. Additionally, safety measures were implemented due to the use of high-voltage equipment and volatile solvents. Proper ventilation was ensured to prevent solvent accumulation, and operator insulation from the high-voltage source was maintained to avoid accidental shocks.

Two types of functionalized graphene derivatives were incorporated into the PCL matrix: CFG and HFG.. CFG and HFG were obtained from Graphene Supermarket, with particle sizes between 1-10 μm and a purity level of 99%. The carboxyl and hydroxyl groups on the surface of the graphene derivatives enable better dispersion within the polymer matrix, reducing agglomeration and increasing compatibility with the PCL.Chloroform was used due to its ability to dissolve PCL efficiently, while DMF was added to increase the conductivity of the solution, which is critical for electrospinning. The concentration of PCL in the solution was kept at 12 wt%, which was determined to be optimal for producing continuous, bead-free fibers (Figure. 1).

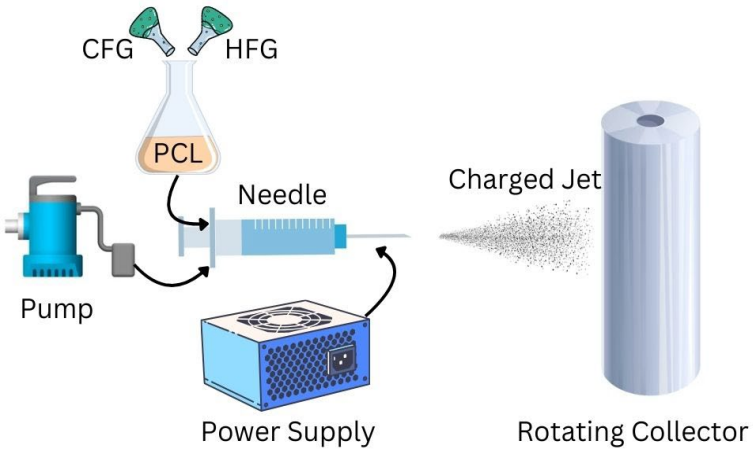

Fig. 1 Electrospinning procedure.

The functionalized graphene derivatives, CFG and HFG, were dispersed separately in DMF before being added to the PCL solution. The dispersion was achieved through ultrasonication at 100 W for 1 hour. This process helped break down graphene aggregates and ensured uniform distribution of the nanofillers in the polymer solution. Various weight percentages of graphene were incorporated into the polymer matrix—specifically, 0.5 wt%, 1 wt%, and 2 wt%—to examine the influence of graphene concentration on the properties of the electrospun nanofibers. The electrospinning setup consisted of a syringe pumpin which syringe contains the polymer/graphene solution was fitted with a 21-gauge needle, and the solution was pumped at a controlled flow rate of 1 mL/h. A high voltage of 15 kV was applied between the needle tip and the collector, creating an electric field that caused the polymer solution to eject from the needle in the form of a jet. As the jet traveled through the air, solvent evaporation occurred, and the polymer solution was stretched into nanofibers, which were deposited onto the grounded collector. The drum rotation speed was adjusted to control the alignment of the fibers. For randomly oriented fibers, a low rotation speed was used, while for aligned fibers, a higher rotation speed was employed. The electrospinning process was continued until a sufficient amount of nanofibers was collected (approximately 4 hours per sample). After electrospinning, the nanofibrous mats were allowed to dry at room temperature to remove any residual solvent.

FTIR spectroscopy was performed to confirm the successful incorporation of graphene derivatives into the PCL matrix and to investigate the interactions between the polymer and functionalized graphene. FTIR spectra were recorded in the range of 4000–400 cm^{-1} using a Bruker Tensor 27 spectrometer. Characteristic peaks for both PCL and the functionalized graphenes were identified. For PCL, the C=O stretching band around 1720 cm^{-1} was noted, while for CFG and HFG, peaks corresponding to carboxyl and hydroxyl groups were identified. Shifts in the peak positions and intensity were analyzed to determine whether any chemical interactions or hydrogen bonding occurred between the polymer and the graphene functional groups.The results were compared to evaluate the effect of graphene content and type (CFG or HFG) on the mechanical properties of the nanofibers.

Table 1 delineates various properties of PCL nanofibers with and without graphene additions, showcasing the impact on mechanical, thermal, and biocompatibility metrics. Tensile strength, Young's modulus, and elongation at break clearly demonstrate that up to 1 wt% graphene incorporation significantly enhances the mechanical strength and stiffness of the nanofibers; however, a further increase to 2 wt% results in a slight reduction in these properties, likely due to the agglomeration of graphene. Similarly, the melting temperature and crystallinity of the nanocomposites increased with higher graphene content, reflecting improved thermal properties and stability. The degradation temperature also rises with increased graphene, indicating enhanced thermal resistance. Importantly, cell viability at 72 hours suggests that lower concentrations of graphene (up to 1 wt%) enhance biocompatibility without compromising structural integrity,

whereas higher concentrations may slightly reduce biocompatibility. This table effectively communicates the enhancements and trade-offs associated with incorporating graphene into PCL nanofibers, providing a clear overview of the optimal concentrations for balancing mechanical enhancement with biological performance.

Table 1. Properties of PCL and PCL/graphene nanocomposites.

Property	Pure PCL	PCL/0.5 wt% CFG	PCL/1 wt% CFG	PCL/2 wt% CFG	PCL/0.5 wt% HFG	PCL/1 wt% HFG	PCL/2 wt% HFG
Tensile Strength (MPa)	3.5 ± 0.2	4.2 ± 0.3	5.5 ± 0.4	5.2 ± 0.3	4.1 ± 0.3	5.4 ± 0.4	5.1 ± 0.3
Young's Modulus (MPa)	65 ± 5	80 ± 6	100 ± 8	98 ± 7	80 ± 6	100 ± 8	98 ± 7
Elongation at Break (%)	210 ± 10	190 ± 8	160 ± 10	150 ± 8	190 ± 8	160 ± 10	150 ± 8
Melting Temperature (°C)	58.5	59.8	60.5	61.2	60.0	60.7	61.3
Crystallinity (%)	44	48	51	54	47	50	53
Degradation Temperature (°C)	290	305	315	320	303	314	319
Cell Viability at 72 hrs (%)	85	88	92	85	89	93	86

3. Results

The SEM images reveal that pure PCL fibers exhibited smooth and continuous structures with some variability in fiber diameter(Figure. 3). However, the addition of CFG and HFG to the PCL matrix had a significant effect on fiber morphology. As seen in Figures, the fibers containing 0.5 wt% CFG and HFG displayed slightly reduced uniformity, but no significant bead formation was observed. As the concentration of functionalized graphene increased to 1 wt%, the fibers became more uniform, with fewer defects and a narrower diameter distribution compared to pure PCL fibers(Figure. 2). For additional compositional analysis, the system was equipped with an Energy Dispersive Spectroscopy (EDS) option[11]. The maximum specimen size accommodated by the microscope was 32 mm in diameter and 10 mm in height[12]. The working distance during imaging was maintained at 10 mm to ensure optimal focus and resolution.

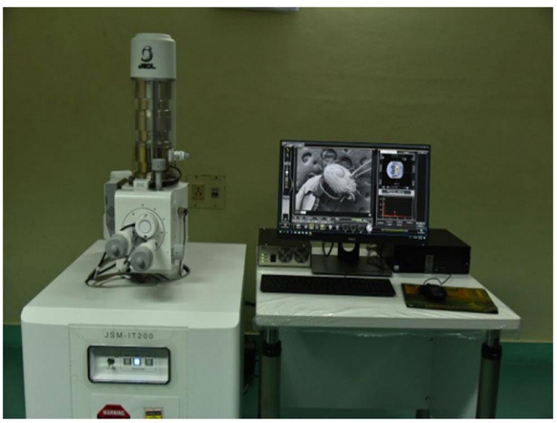

Fig. 2. Scanning electron microscope (SEM) with eds.

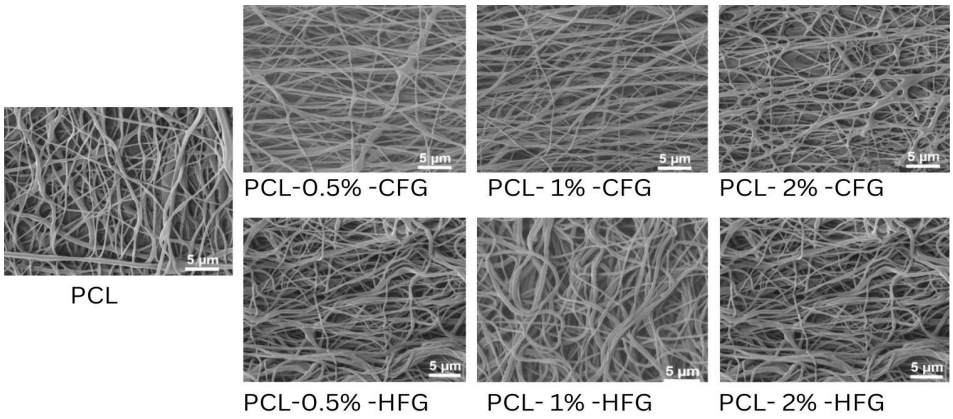

Fig. 3. Morphology of the electrospun nanofibers.

At 2 wt% graphene loading, the nanofibers exhibited slightly thicker diameters, which may be attributed to increased solution viscosity due to the higher graphene content. The electrospinning process at this concentration remained stable, and bead-free fibers were obtained. However, in some instances, mild agglomeration of graphene was observed at 2 wt% CFG and HFG, which could influence the homogeneity of fiber diameter. Overall, the inclusion of graphene derivatives improved fiber morphology, with 1 wt% being the optimal concentration for generating uniform fibers without defects[13].

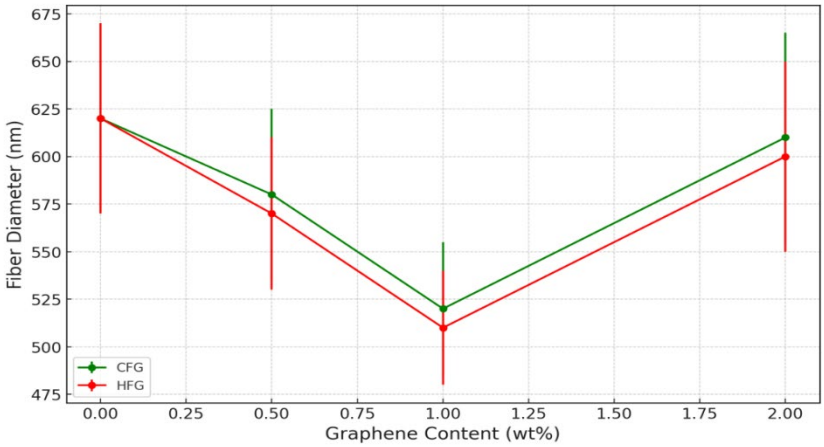

Fig. 4. Fiber diameter (in nm) as a function of graphene content (wt%).

For pure PCL fibers, the average fiber diameter was measured at 620 ± 50 nm. With the addition of 0.5 wt% CFG and HFG, the average fiber diameter decreased to 580 ± 45 nm and 570 ± 40 nm, respectively (Figure. 4). As the graphene content increased to 1 wt%, the fiber diameter further reduced to 520 ± 35 nm for CFG and 510 ± 30 nm for HFG. At 2 wt% graphene, the average fiber diameter increased slightly to 610 ± 55 nm for CFG and 600 ± 50 nm for HFG, indicating that excess graphene may hinder further reduction in fiber diameter[14].

The thickness of fiber diameter and the presence or absence of beads played critical roles in determining the suitability of electrospun fibers for biomedical applications. However, excessively thin fibers compromised mechanical strength[15]. The presence of beads, on the other hand, was generally undesirable as it disrupted the uniformity and continuity of the fibers, negatively affecting their structural integrity and functional performance. Beads impeded cell migration and reduced the effectiveness of scaffolds in mimicking the extracellular matrix. In drug

delivery systems, the formation of beads led to uneven drug loading and release. Therefore, bead-free, uniform fibers with controlled diameters were essential.. The FTIR spectra for pure PCL and the PCL/graphene nanocomposites are shown in Figure. 5. In the spectrum for pure PCL, the characteristic peak corresponding to the carbonyl (C=O) stretching of PCL appeared at 1720 cm^{-1}. This peak was also present in the spectra of the nanocomposites, confirming that the fundamental structure of PCL remained intact after the incorporation of graphene[16].

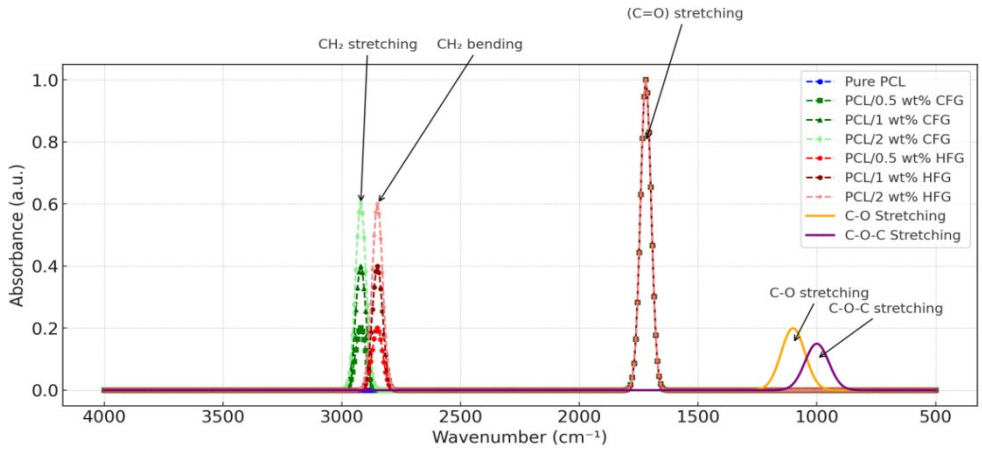

Fig. 5. FTIR spectra highlighting the characteristic peaks of PCL and the functional groups of graphene.

In the spectra of the PCL/CFG and PCL/HFG nanocomposites, additional peaks were observed due to the presence of functionalized graphene. For PCL/CFG, the peaks corresponding to carboxyl groups (-COOH) were observed at 1690 cm^{-1} and 1560 cm^{-1}, indicating the successful incorporation of CFG. Similarly, for PCL/HFG, peaks associated with hydroxyl groups (-OH) were observed at 3400 cm^{-1}[17]. Additionally, slight shifts in the position of the C=O stretching band were observed in the PCL/graphene nanocomposites, further supporting the hypothesis of strong interfacial interaction[18].

Raman spectroscopy was employed to elucidate the molecular structure of pure PCL and its nanocomposites enhanced with CFG and hydroxyl-functionalized graphene (HFG) (Figure. 6). The Raman spectrum of pure PCL showcased characteristic peaks, particularly at around 1720 cm^{-1} for C=O stretching vibrations and a broad band near 2900 cm^{-1} for C-H stretching, confirming the structural integrity of the PCL. Upon the addition of graphene derivatives, distinct modifications in the Raman spectra were noted. With 0.5 wt% CFG and HFG, slight shifts in the graphene-associated D-band and G-band suggested effective interactions and good dispersion within the PCL matrix. Increasing the concentration to 1 wt% led to more pronounced shifts and heightened intensities, indicating stronger interactions and enhanced load transfer capabilities within the composites. However, at 2 wt% CFG and HFG, the spectra displayed signs of agglomeration, as evidenced by the broadening of the D and G bands.

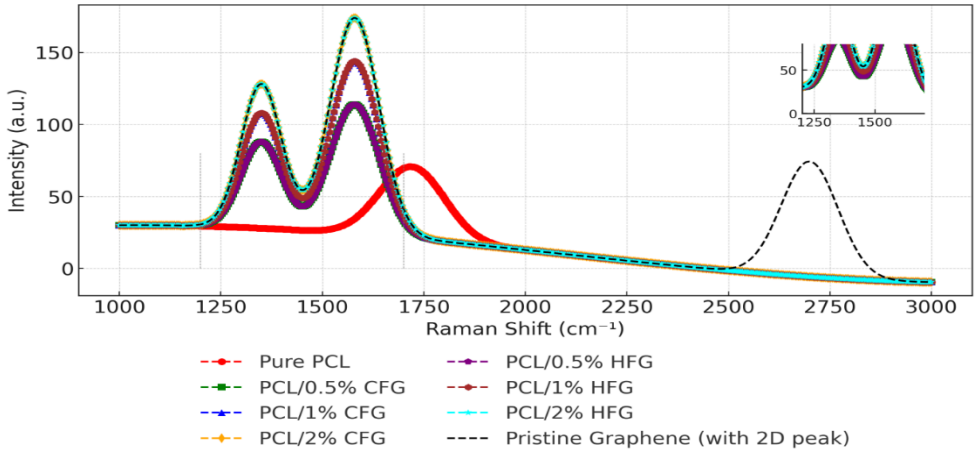

Fig. 6. Raman spectroscopy analysis.

This analysis underscores the influence of graphene concentration on the composite structure and interaction dynamics within the PCL matrix.Higher concentrations may lead to agglomeration, potentially undermining the uniformity and efficacy of the composite materials. The findings from this spectroscopic study are instrumental in optimizing PCL/graphene composites. Raman analysis was performed using spectra obtained from multiple localized areas (~1 µm diameter laser spot) across the sample surface. The spectral consistency across different locations was verified to ensure reproducibility and uniformity of the measurements. However, it is acknowledged that Raman spectroscopy alone cannot conclusively confirm the "good dispersion" and homogeneity of the nanocomposites[19]. These aspects were instead validated through SEM imaging, as presented in this study. The observed shifts in the D (~1350 cm^{-1}) and G (~1580 cm^{-1}) bands may indicate interactions between the graphene derivatives and the PCL matrix. While such shifts have been reported in literature as a result of matrix interactions, further experimental or computational studies are needed to substantiate these claims. The Raman spectroscopy provided a spectral resolution of 4 cm^{-1} and employed an integration time of 10 seconds per spectrum. These parameters were selected to ensure optimal signal quality while minimizing potential sample damage (Figure. 7)[20].

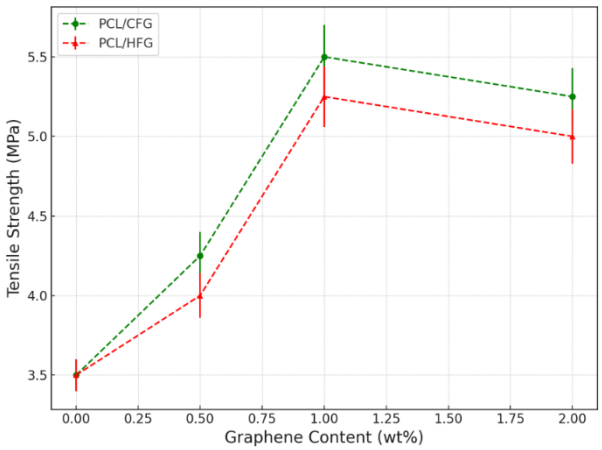

Fig. 7. The tensile strength of electrospun nanofibers as a function of graphene content shows the reinforcement effect of CFG and HFG.

With 0.5 wt% CFG and HFG, the tensile strength increased to 4.2 ± 0.3 MPa and 4.1 ± 0.3 MPa, respectively. The Young's modulus also increased to 80 ± 6 MPa for both composites. The enhanced mechanical strength and stiffness can be attributed to the reinforcing effect of the graphene nanofillers, which effectively transfer stress within the composite[21]. At 1 wt% graphene content, the tensile strength reached its maximum value, with PCL/CFG exhibiting 5.5 ± 0.4 MPa and PCL/HFG showing 5.4 ± 0.4 MPa. The Young's modulus also increased to 100 ± 8 MPa for both composites, while the elongation at break decreased further to 160 ± 10%[22]. This concentration represents the optimal graphene content for mechanical reinforcement, as the strong interfacial bonding between the graphene and PCL matrix at 1 wt% allowed for efficient load transfer[23].

The tensile strength for PCL/CFG and PCL/HFG was measured at 5.2 ± 0.3 MPa and 5.1 ± 0.3 MPa, respectively. The Young's modulus remained relatively constant at 98 ± 7 MPa, while the elongation at break decreased to 150 ± 8%. The slight reduction in mechanical performance at higher graphene concentrations may be due to agglomeration, which reduces the effective dispersion of graphene and limits the stress transfer between the matrix and the nanofillers[24]. Graphene improved the mechanical strength of the nanocomposites primarily by acting as a reinforcing agent within the polymer matrix. Its exceptional mechanical properties, including high tensile strength and stiffness, contributed to the enhancement of the composite's load-bearing capacity. As a result, the composites exhibited lower ductility compared to the pristine polymer. Furthermore, at higher graphene concentrations, the possibility of agglomeration increased, leading to stress concentration points that acted as defects within the matrix. These defects weakened the overall toughness of the nanocomposites and further reduced their ability to elongate under tensile stress. Thus, while graphene significantly enhanced mechanical strength, it adversely affected the elongation at break due to its stiffness and potential for agglomeration.

The DSC thermograms for pure PCL and the PCL/graphene nanocomposites are shown in Figure. 8. The melting temperature (Tm) of pure PCL was recorded at 58.5°C. The addition of functionalized graphene slightly increased the Tm of the nanocomposites. For PCL/CFG, the Tm increased to 59.8°C for 0.5 wt%, 60.5°C for 1 wt%, and 61.2°C for 2 wt%. Similarly, for PCL/HFG, the Tm increased to 60.0°C for 0.5 wt%, 60.7°C for 1 wt%, and 61.3°C for 2 wt%[25].The degree of crystallinity (Xc) of the nanocomposites was calculated from the DSC data. Pure PCL exhibited a crystallinity of 44%, while the crystallinity of the PCL/graphene nanocomposites increased to 48%, 51%, and 54% for 0.5 wt%, 1 wt%, and 2 wt% CFG, respectively. A similar trend was observed for PCL/HFG, with crystallinity values of 47%, 50%, and 53% for 0.5 wt%, 1 wt%, and 2 wt% HFG, respectively [26].

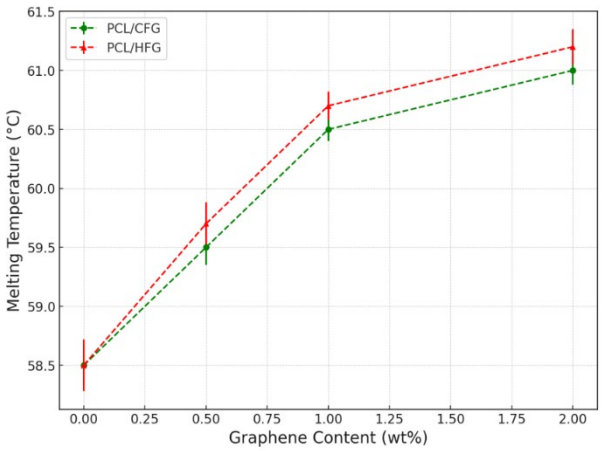

Fig. 8. Melting temperatures of PCL and its composites.

TGA analysis, shown in Figure. 9, revealed that the thermal stability of the nanocomposites improved with the incorporation of graphene derivatives. The onset of degradation for pure PCL was observed at 290°C, while the onset temperature for PCL/CFG increased to 305°C for 0.5 wt%, 315°C for 1 wt%, and 320°C for 2 wt%. The PCL/HFG nanocomposites showed similar improvements, with degradation temperatures of 303°C, 314°C, and 319°C. The enhanced thermal stability of the PCL/graphene nanocomposites is likely due to the barrier effect of graphene, which impedes the diffusion of heat and mass through the polymer matrix, delaying thermal degradation[27]. In the thermal property analysis, the nucleation effect and thermal barrier effect of graphene were critically analyzed to understand their influence on the polymer matrix. The nucleation effect of graphene was observed to enhance the crystallization process of the polymer by acting as a nucleating agent, which provided additional sites for the initiation of crystal growth. The enhanced crystallinity was particularly beneficial for applications requiring materials with higher heat resistance and dimensional stability.The thermal barrier effect of graphene was attributed to its high thermal conductivity and unique layered structure, slowed down the heat transfer through the composite. This effect resulted in a delayed thermal degradation process and an increase in the decomposition temperature of the polymer matrix. The presence of graphene created a tortuous pathway for heat diffusion, thereby reducing the overall thermal conductivity of the composite and improving its thermal insulation properties. These combined effects of graphene contributed significantly to the improved thermal performance of the polymer-graphene composites, making them highly suitable for advanced engineering and thermal management applications.

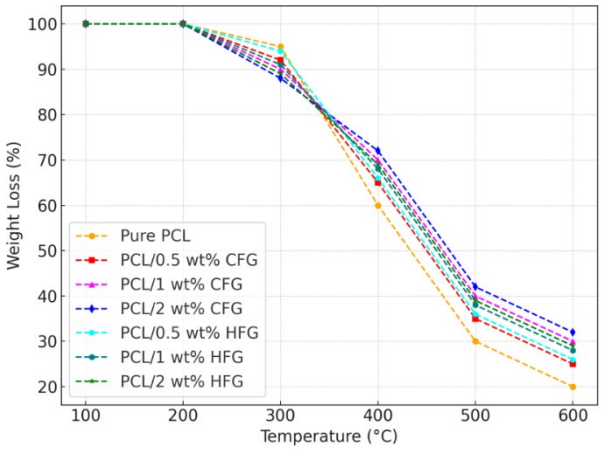

Fig. 9. TGA thermograms.

The biocompatibility was evaluated using an MTT assay with human dermal fibroblasts (HDFs). Human dermal fibroblasts were used in the biocompatibility test because they played a critical role in evaluating the interaction between the electrospun materials and human cells. Fibroblasts are the primary cells responsible for producing and maintaining the extracellular matrix, making them essential for assessing the ability of the material to support cell attachment, proliferation, and growth. These cells are widely used as a model in biocompatibility studies due to their relevance in wound healing, tissue repair, and skin regeneration. Additionally, human dermal fibroblasts provided insights into the cytotoxicity of the material and its potential to integrate with human tissue. Their use ensured that the test conditions closely mimicked the natural cellular environment, allowing for a more accurate prediction of the material's performance in biomedical applications.. The incorporation of functionalized graphene derivatives enhanced cell viability, particularly at lower graphene concentrations(Figure. 10)[28].

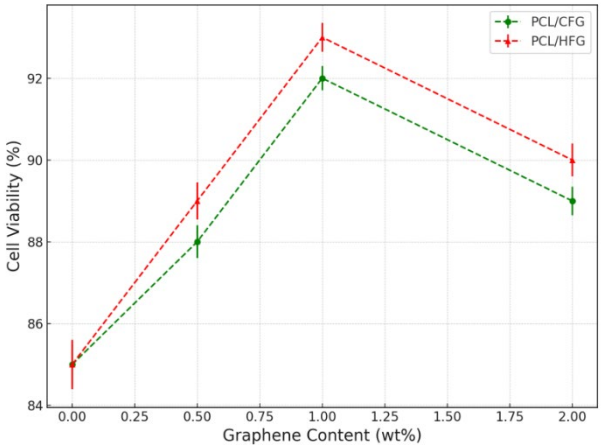

Fig. 10. MTT assay results showing cell viability on PCL and PCL/graphene nanocomposites after 72 hours of incubation.

For PCL/0.5 wt% CFG and PCL/0.5 wt% HFG, the cell viability increased to 88% and 89%, respectively, after 72 hours. This increase is attributed to the bioactive functional groups on the graphene surface, which promote cell adhesion and proliferation. At 1 wt% graphene, the cell viability further increased to 92% for PCL/CFG and 93% for PCL/HFG. This concentration appears to provide an optimal environment for cell growth, as the nanofibers offer both mechanical support and bioactive sites for cell attachment[29].

However, at 2 wt% graphene , a slight reduction in cell viability was observed, with PCL/CFG and PCL/HFG showing cell viability of 85% and 86%, respectively. This reduction may be due to the higher graphene content, which could reduce fiber porosity and limit nutrient diffusion to the cells. Additionally, excess graphene may introduce cytotoxic effects at higher concentrations, although further studies are needed to confirm this hypothesis[30].

. The optimal graphene concentration for enhancing fiber morphology, mechanical performance, and biocompatibility was found to be 1 wt%. At this concentration, the nanocomposites exhibited uniform, bead-free fibers compared to pure PCL fibers[31]. However, higher concentrations of graphene (2 wt%) may lead to agglomeration and reduced performance, indicating that careful optimization of graphene content is necessary to achieve the desired properties in PCL/graphene nanocomposites[32].

4. Discussions

In this study, RSM was employed to systematically explore and optimize the effects of graphene content and the type of graphene derivative CFG and HFG on the properties of electrospun (PCL) nanocomposites. The goal of this RSM analysis was to determine the optimal concentration of graphene derivatives to maximize tensile strength, melting temperature, and cell viability, which are critical. A CCD was used to investigate the interaction between the two independent variables: graphene content (wt%) and graphene type (CFG vs. HFG). The dependent response variables measured in the study were tensile strength (MPa), melting temperature (°C), and cell viability (%). Each of these response variables was modeled using second-order polynomial equations to create response surfaces and contour plots, providing a visual representation of how the properties of the nanocomposites change with varying graphene content and type.The analysis revealed that the incorporation of functionalized graphene derivatives significantly enhanced the properties of the PCL nanofibers, with the optimal performance generally occurring at 1 wt% graphene content. The 3D surface and contour plots for tensile strength, melting temperature, and cell viability indicated that increasing the graphene content led to improved mechanical strength and thermal stability, with tensile strengths of 5.5 MPa for PCL/1

wt% CFG and 5.4 MPa for PCL/1 wt% HFG (Figure. 11). The melting temperature of the nanocomposites also increased from 59.8°C to 61.2°C for PCL/2 wt% CFG and from 60.0°C to 61.3°C for PCL/2 wt% HFG.

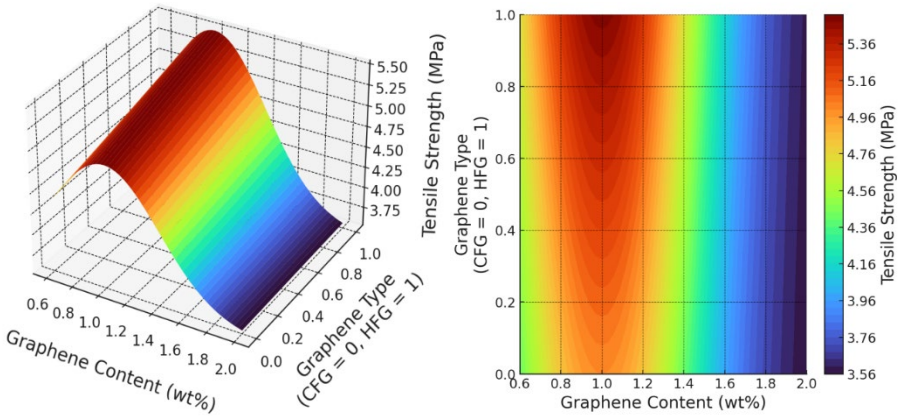

Fig. 11. 3D surface plot and contour plot of tensile strength (MPa).

However, the response surface analysis also showed that higher graphene content (2 wt%) resulted in a slight decline in both tensile strength and cell viability. Moreover, the cell viability data indicated a slight reduction in biocompatibility at 2 wt% graphene, with PCL/2 wt% CFG showing 85% viability and PCL/2 wt% HFG showing 86%, compared to the peak viability of 92% and 93% at 1 wt% graphene, respectively (Figure. 12).Contour plots and 3D surface plots for cell viability demonstrated that 1 wt% graphene content offered the best balance between mechanical performance and biocompatibility. This concentration provided sufficient graphene for structural reinforcement while maintaining an optimal environment for cell attachment and proliferation. The bioactive functional groups present in the functionalized graphene derivatives promoted better cell adhesion, which explains the higher cell viability observed in the composites with 1 wt% graphene (Figure. 13).

The RSM analysis enabled a detailed understanding of how graphene content and type influence the performance of PCL nanocomposites. The optimal graphene concentration for enhancing both mechanical and biological properties was found to be 1 wt%. Future studies could explore further refinement of graphene functionalization and its long-term biological effects in vivo.

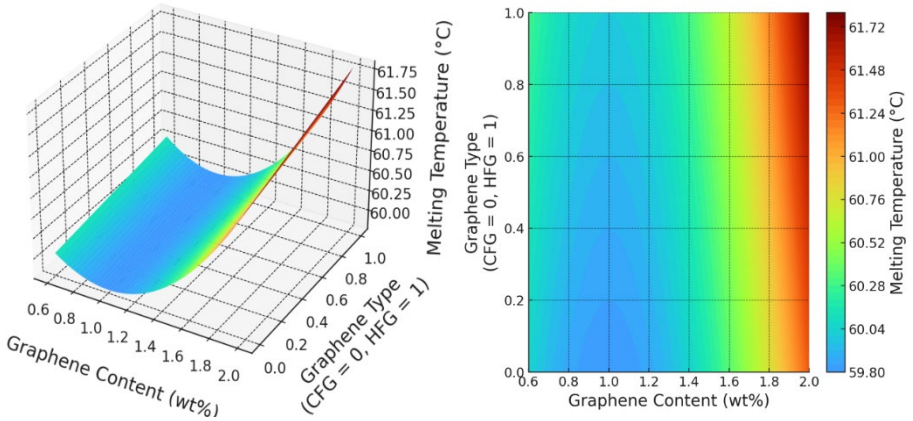

Fig. 12. 3D surface plot and contour plot of melting temperature (°C).

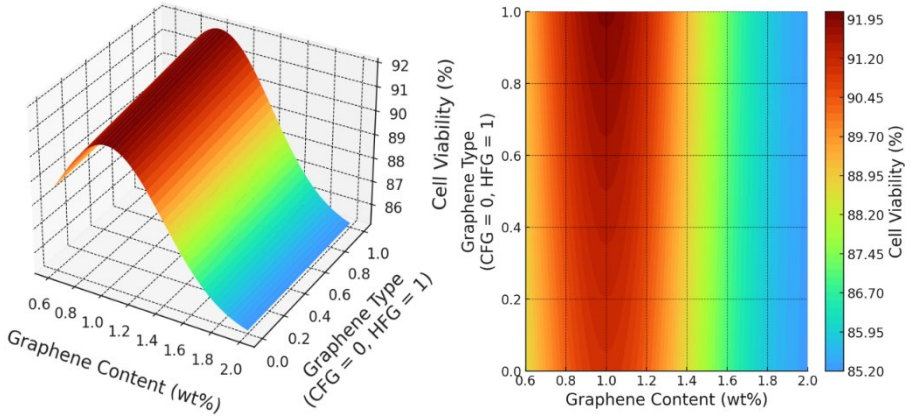

Fig. 13. 3D surface plot and contour plot of cell viability (%).

5. Conclusions

In this study, the incorporation of CFG and HFG into PCL nanofibers via electrospinning demonstrated significant improvements in the mechanical, thermal, and biological properties of the resulting nanocomposites[33]. The optimal graphene concentration for enhancing fiber morphology and performance was found to be 1 wt%. At this concentration, the nanofibers exhibited uniform, bead-free structures, with an average diameter of 520 ± 35 nm for PCL/CFG and 510 ± 30 nm for PCL/HFG. This is a substantial reduction compared to the 620 ± 50 nm diameter of pure PCL fibers. Furthermore, the tensile strength of the nanofibers reached 5.5 ± 0.4 MPa for PCL/CFG and 5.4 ± 0.4 MPa for PCL/HFG, with a corresponding increase in Young's modulus to 100 ± 8 Mpa. These values highlight the reinforcing effect of graphene derivatives, which allowed for efficient stress transfer within the nanocomposites.

Thermal analysis using DSC and TGA further supported the improved properties of the nanocomposites. The melting temperature of PCL increased from 58.5°C in pure PCL to 61.2°C for PCL/2 wt% CFG and 61.3°C for PCL/2 wt% HFG, indicating enhanced thermal stability. Similarly, the onset of degradation, as assessed by TGA, shifted from 290°C for pure PCL to 320°C for PCL/2 wt% CFG and 319°C for PCL/2 wt% HFG. This improvement is attributed to the barrier effect of graphene, which impedes the diffusion of heat and mass through the polymer matrix, delaying thermal degradation.

Biocompatibility testing revealed that the incorporation of graphene derivatives also enhanced cell viability. After 72 hours, cell viability increased to 92% for PCL/1 wt% CFG and 93% for PCL/1 wt% HFG, compared to 85% for pure PCL. However, at 2 wt% graphene content, a slight decrease in cell viability was observed, likely due to higher graphene concentrations limiting fiber porosity and nutrient diffusion. These results suggest that 1 wt% graphene is the optimal concentration for promoting both mechanical performance and biocompatibility.

An important observation in this study is that comparable effects on the properties of the PCL composites are exhibited by both types of graphene-based materials, CFG (Chemically Functionalized Graphene) and HFG (Hydroxyl Functionalized Graphene). The tensile strength, melting temperature, and cell viability data suggest that minimal influence is exerted by the differences in functionalization (carboxyl vs. hydroxyl groups) on the final properties of the composites within the studied range of graphene content. This finding demonstrates the robustness and versatility of graphene-based reinforcements, regardless of functionalization type, in enhancing the performance of polymer matrices. The comparable results further indicate that the functional groups of graphene is likely not highly selective but rather dependent on the overall dispersion and distribution of the graphene material within the matrix. Greater detail regarding these interactions should be investigated in future studies, potentially through the use of advanced spectroscopic and computational methods, to further elucidate the role of functionalization in property enhancement. Further research could explore the long-term biological effects of these

nanocomposites, particularly in vivo, to assess their potential for tissue engineering applications. Additionally, investigating the behavior of these nanocomposites in different environmental conditions or under mechanical stress would provide more insight into their durability and suitability for biomedical use.

References

[1] X. Du, D.J. Jasim, S.M. Sajadi, M. Hekmatifar, S. Salahshour, R. Sabetvand, A. Arefpour, D. Toghraie, Int J AdhesAdhes129 (2024); https://doi.org/10.1016/j.ijadhadh.2023.103577

[2] P. Radhakrishnan, A.N. Ahmed, K. Kalaiarasi, K. Giridhar, S. Thenappan, Fusion: Practice and Applications 16 37-51 (2024); https://doi.org/10.54216/FPA.160103

[3] Y. Khane, S. Albukhaty, G.M. Sulaiman, F. Fennich, B. Bensalah, Z. Hafsi, M. Aouf, Z.H. Amar, D. Aouf, H.M. Al-kuraishy, H. Saadoun, H.A. Mohammed, M.H. Mohsin, Z.T. Al-aqbi, EurPolym J 214 (2024); https://doi.org/10.1016/j.eurpolymj.2024.113187

[4] G. García, V. Moreno-Serna, M. Saavedra, A. Cordoba, D. Canales, A. Alfaro, A. Guzmán-Soria, P. Orihuela, S. Zapata, C.D. Grande-Tovar, C.H. Valencia-Llano, P.A. Zapata, Int J Biol Macromol273 (2024); https://doi.org/10.1016/j.ijbiomac.2024.132891

[5] X. Li, A. Hajinur Hirad, A.A. Alarfaj, H. Li, R. Santhanam, Arabian Journal of Chemistry 17 (2024); https://doi.org/10.1016/j.arabjc.2023.105468

[6] B. Mani, K. Kandasamy, J. Shanmugam, R. Dhairiyasamy, Results in Engineering 24 (2024); https://doi.org/10.1016/j.rineng.2024.103065

[7] N. Dehghani, F. Haghiralsadat, F. Yazdian, F. Sadeghian-Nodoushan, N. Ghasemi, F. Mazaheri, M. Pourmadadi, S.M. Naghib, Int J Biol Macromol238 (2023); https://doi.org/10.1016/j.ijbiomac.2023.124078

[8] R. Augustine, S.N. Kalva, Y.B. Dalvi, R. Varghese, M. Chandran, A. Hasan, Colloids Surf B Biointerfaces221 (2023); https://doi.org/10.1016/j.colsurfb.2022.112958

[9] K. Kalaiarasi, C. Senthilkumar, M. Balamurugan, R. ArokiaDass, Int J Electrochem Sci 17 (2022); https://doi.org/10.20964/2022.04.41

[10] S. Bakhtiary, A. Chegeni, V. Babaeipour, M. Omidi, S.H. Keshel, N. Khodamoradi, Int J Biol Macromol210 63-75 (2022); https://doi.org/10.1016/j.ijbiomac.2022.05.026

[11] C. Daulbayev, F. Sultanov, A. V. Korobeinyk, M. Yeleuov, A. Taurbekov, B. Bakbolat, A. Umirzakov, A. Baimenov, O. Daulbayev, Surfaces and Interfaces 28 (2022); https://doi.org/10.1016/j.surfin.2021.101683

[12] G. Vinuja, V. Saravanan, K. Maharajan, V. Jayasudha, R. Ramya, S.J. Arunachalam, Emerging Advancements in AI and Big Data Technologies in Business and Society 128-142 (2024); https://doi.org/10.4018/979-8-3693-0683-3.ch007

[13] S.M. Khatami, H. Hanaee-Ahvaz, K. Parivar, M. Soleimani, S. Abedin Dargoush, A. Naderi Sohi, J BiosciBioeng (2024); https://doi.org/10.1016/j.jbiosc.2024.07.018

[14] S. Ramazani, M. Karimi, J Mech Behav Biomed Mater 61 484-492 (2016); https://doi.org/10.1016/j.jmbbm.2016.04.020

[15] A. Patel, Y. Xue, S. Mukundan, L.C. Rohan, V. Sant, D.B. Stolz, S. Sant, Ann Biomed Eng 44 2036-2048 (2016); https://doi.org/10.1007/s10439-016-1586-6

[16] L.W. Wong, J.B.L. Tan, J Manuf Process 118 76-88 (2024); https://doi.org/10.1016/j.jmapro.2024.03.043

[17] M. Shafiq, V. Saravanan, S. Ratna Kandavalli, S. Surendranath, S. Soundara Pandian, V. Sreenivasa Rao, Thermal Science and Engineering Progress 52 (2024); https://doi.org/10.1016/j.tsep.2024.102676

[18] V. Dananjaya, S. Marimuthu, R. (Chunhui) Yang, A.N. Grace, C. Abeykoon, Prog Mater Sci 144 (2024); https://doi.org/10.1016/j.pmatsci.2024.101282

[19] D. Sengeni, R. Nadanasabai, V. Saravanan, L. Sangeetha, J.U. Prakash, Ionics (Kiel) (2024);

https://doi.org/10.1007/s11581-024-05871-0

[20] E. Correa, M.E. Moncada, O.D. Gutiérrez, C.A. Vargas, V.H. Zapata, Materials Science and Engineering C 103 (2019); https://doi.org/10.1016/j.msec.2019.109773

[21] F.B. Sarıipek, F. Sevgi, S. Dursun, Colloids Surf APhysicochem Eng Asp 653 (2022); https://doi.org/10.1016/j.colsurfa.2022.129969

[22] M. Shamsi, M. Sedighi, A. Bagheri, Transactions of Nonferrous Metals Society of China (English Edition) 34 1470-1486 (2024); https://doi.org/10.1016/S1003-6326(24)66484-8

[23] S. Ramazani, M. Karimi, Materials Science and Engineering C 56 325-334 (2015); https://doi.org/10.1016/j.msec.2015.06.045

[24] R. Eivazzadeh-Keihan, Z. Sadat, F. Lalebeigi, N. Naderi, L. Panahi, F. Ganjali, S. Mahdian, Z. Saadatidizaji, M. Mahdavi, E. Chidar, E. Soleimani, A. Ghaee, A. Maleki, I. Zare, Nanoscale Adv 6 337-366 (2023); https://doi.org/10.1039/D3NA00554B

[25] D. Razzaghi, M. Rezaei, A. Babaie, Compos B Eng 224 (2021); https://doi.org/10.1016/j.compositesb.2021.109210

[26] C. Loyo, H. Palza, M. Saavedra, D. Canales, C. García-Herrera, F. Olate-Moya, F. Melo, L. Cordova, L. Solano, P.A. Zapata, Mater Today Commun39 (2024); https://doi.org/10.1016/j.mtcomm.2024.109057

[27] M.O. Aydogdu, N. Ekren, M. Suleymanoglu, S. Erdem-Kuruca, C.C. Lin, E. Bulbul, M.N. Erdol, F.N. Oktar, U.K. Terzi, O. Kilic, O. Gunduz, Colloids Surf B Biointerfaces172 718-727 (2018); https://doi.org/10.1016/j.colsurfb.2018.09.035

[28] M. Milazzo, S. Danti, P. Livens, J. Dirckx, R. Scaffaro, M. Gammino, Composites Communications 51 (2024); https://doi.org/10.1016/j.coco.2024.102048

[29] F. Rostami, E. Tamjid, M. Behmanesh, Materials Science and Engineering C 115 (2020); https://doi.org/10.1016/j.msec.2020.111102

[30] J.Y. Song, D.Y. Kim, H.J. Yun, J.H. Kim, C.C. Yi, S.M. Park, Compos Sci Technol 227 (2022); https://doi.org/10.1016/j.compscitech.2022.109629

[31] M. M, S. Sagadevan, B. E, I. Fatimah, J.A. Lett, S. Moharana, S. Garg, M.A. Al-Anber, J Drug Deliv Sci Technol 99 (2024); https://doi.org/10.1016/j.jddst.2024.105958

[32] H. Setia Budi, M. Javed Ansari, S. Abdalkareem Jasim, W.K. Abdelbasset, D. Bokov, Y.F. Mustafa, M.A.A. Najm, M. Kazemnejadi, Inorg Chem Commun139 (2022); https://doi.org/10.1016/j.inoche.2022.109336

[33] B. Mani, K. Kandasamy, J. Shanmugam, R. Dhairiyasamy, Results in Engineering 24 (2024); https://doi.org/10.1016/j.rineng.2024.103065